Colloids and Surfaces B: Biointerfaces 222 (2023) 113019

Contents lists available at ScienceDirect

Colloids and Surfaces B: Biointerfaces

journal homepage: www.elsevier.com/locate/colsurfb

Effect of surface functionalization and loading on the mechanical properties of soft polymeric nanoparticles prepared by nano-emulsion templating

Aurora Dols-Perez [a,b,c,d,*], Cristina Fornaguera [a,b,e], Natalia Feiner-Gracia [a,b], Santiago Grijalvo [a,b], Conxita Solans [a,b,1], Gabriel Gomila [c,d,1]

[a] Institute of Advanced Chemistry of Catalonia (IQAC-CSIC), C/Jordi Girona 18–26, 08034 Barcelona, Spain
[b] Biomedical Research Networking Center in Bioengineering, Biomaterials and Nanomedicine (CIBER-BBN), Spain
[c] Institut de Bioenginyeria de Catalunya (IBEC), C/ Balidiri i Reixac 15–21, 08028 Barcelona, Spain
[d] Departament of Electronics and Biomedical Engineering, Universitat de Barcelona, C/ Martí i Franquès 1, 08028 Barcelona, Spain
[e] Grup d'Enginyeria de Materials (Gemat) – Institut Químic de Sarrià (IQS) – Universitat Ramon Llull (URL), Barcelona, Spain

ARTICLE INFO

Keywords:
Polymeric nanoparticles
Mechanics of nanoparticles
AFM
Nanoparticle functionalization
Nanomedicine
Young's modulus

ABSTRACT

Drug and gene delivery systems based on polymeric nanoparticles offer a greater efficacy and a reduced toxicity compared to traditional formulations. Recent studies have evidenced that their internalization, biodistribution and efficacy can be affected, among other factors, by their mechanical properties. Here, we analyze by means of Atomic Force Microscopy force spectroscopy how composition, surface functionalization and loading affect the mechanics of nanoparticles. For this purpose, nanoparticles made of Poly(lactic-co-glycolic) (PLGA) and Ethyl cellulose (EC) with different functionalizations and loading were prepared by nano-emulsion templating using the Phase Inversion Composition method (PIC) to form the nano-emulsions. A multiparametric nanomechanical study involving the determination of the Young's modulus, maximum deformation and breakthrough force was carried out. The obtained results showed that composition, surface functionalization and loading affect the nanomechanical properties in a different way, thus requiring, in general, to consider the overall mechanical properties after the addition of a functionalization or loading. A graphical representation method has been proposed enabling to easily identify mechanically equivalent formulations, which is expected to be useful in the development of soft polymeric nanoparticles for pre-clinical and clinical use.

1. Introduction

The possibility to create biocompatible and biodegradable carriers with greater efficacy and reduced toxicity, in comparison with traditional formulations, has increased notably the interest in polymeric nanoparticles (NP) as drug and gene delivery systems [1–3]. NPs should accomplish certain characteristics regarding their size, biocompatibility, charge and composition to be able to reach the site of action and release the cargo at the required kinetics. Biodistribution, cellular uptake, endocytic pathway and final intracellular localization have been proven to be dependent on the nanocarriers' size, shape, lipophilicity and surface characteristics as porosity or texture [4–9].

In recent years the interest in other factors, such as the nanomechanical properties, has increased notably although still little is known. Nanomechanical parameters, such as stiffness, Young's modulus, rupture force or maximum deformability, among others, define and quantify the deformability of a material, their ability to squeeze or to resist its rupture. So, nanomechanical properties define the behavior of NPs and their resistance against mechanical stress and can influence the lifetime of the nanoparticle in storage as well as in physiological fluids, and thus, compromise the bioavailability of encapsulated active ingredients. Apart from the mechanical stress produced during the fabrication and administration, NPs face different threats during their delivery that can be also affected by their administration route. In intravenous delivery, NPs are exposed to adsorption of proteins during circulation, shear stress due to bloodstream fluidics, interaction

Abbreviations: AFM, Atomic Force Microscopy; BBB, Blood-Brain Barrier; EC, Ethyl cellulose; NP, Nanoparticle; PIC, Phase Inversion Composition method; PLGA, Poly (lactic-co-glycolic acid).

* Correspondence to: Institut de Bioenginyeria de Catalunya, C/Baldiri i Reixac 15-21, 08028 Barcelona, Spain.
E-mail address: adols@ibecbarcelona.eu (A. Dols-Perez).

[1] contributed equally.

https://doi.org/10.1016/j.colsurfb.2022.113019
Received 29 July 2022; Received in revised form 3 November 2022; Accepted 10 November 2022
Available online 12 November 2022

with immune system cells, organs filtration [10–16]. In addition, to perform their activity in the target tissues, nanoparticles are also affected by extravasation to the tissue and the final cell internalization [10–16]. Moreover, less invasive administration routes, which are gaining interest recently, add other mechanical stress sources due to the presence of mucosa. In the case of tumors, cell proliferation and impaired lymphatic drainage increases the fluid pressure in their inside [17]. In all of them mechanics can define the deformability of the NP, the ability to squeeze or to resist but also the liberation of the therapeutic agent.

In the last years the role of NP mechanics has started to be elucidated. Stiffer NPs have been associated with greater penetration rates than softer NPs [18–22]. Applied coarse-grained molecular dynamics studies associated this phenomenon to the larger free energy barrier required for internalization of softer NPs [23]. But, at the same time, it has been demonstrated that the mechanical properties can affect the NPs circulation time, being soft NPs greatly persistent. Some publications attributed this fact to a distinct phagocytosis uptake compared with stiff NPs [24,25]. A recent study also remarked the importance of nanoparticle stiffness on uptake and transcytosis at the blood-brain barrier (BBB) suggesting opposing effects as a function of the carrier characteristics [26]. In other studies, the NP's Young modulus and deformability was linked to spleen accumulation of stiff NPs and, in turn, lower blood circulation times, information that can be also valuable to treat spleen or liver tumors [25,27]. In the case of tumors, in parallel to the phenomena mentioned above, some studies linked the mechanics of NPs to their penetration depth, being softer NPs the ones exhibiting higher penetration rates [25,28]. On the other hand, other works described that it is necessary an equilibrium between the excessive deformation of the shape of NPs with low Young's modulus and the absence of deformation of NPs with high values, being NPs with a semielastic response the ones with better results for pancreatic cell tumor spheroids [29]. Additionally, it has been described that critical barriers for tumor or mucosal delivery can be overcome by modifying the rigidity of NP [29]. Taking into account these evidences and in order to study deeper these phenomena, specific approaches are being developed to get information on the force exerted on NP during cellular uptake [30,31] and the adherence of NPs to the cellular surface [32].

Given the relevance of the mechanical properties of polymeric NPs, new procedures are being studied in order to modify or reliably control them. Recently, hydration has demonstrated to influence the mechanical properties of poly(lactic) (PLA) and poly(lactic-co-glycolic) acid (PLGA) NPs by a 30-fold reduction of the Young's modulus at 37 ºC [33]. In fact, the hydration degree of hydrogels has been shown to be a good and simple way to modify their elasticity [34]. Other options to efficiently tune NP rigidity is to change the level of cross-linking in polymeric and hydrogel NPs [35–38]. A recent study has succeeded in tuning the mechanical properties of nanocarriers without changing its chemistry [39]. In that case, authors created elasticity-tunable nanocarriers based on self-assembly oleanolic acid with different rigidities and demonstrated the differences in their biological activities such as endocytosis and permeation.

Despite these new findings, the role of certain elements in the nanomechanical properties of polymeric NPs remain unexplored. Among them the effect of surface functionalization and loading, key to make NPs functional as therapeutic or diagnostic agents, remain unclear. Here, we precisely address these aspects.

To carry out this investigation we produced polymeric nanoparticles of interest in biomedical application by nano-emulsion templating, preparing the nano-emulsion by the low-energy Phase Inversion Composition (PIC) method [40,41]. This production procedure has the unique ability to allow, in a fully controllable way, modifying the inner part of the NPs, functionalizing their surface, or changing their composition; enabling the obtention of unambiguous results. The use of PIC emulsification method combined with nano-emulsion templating allows to tune the components (e.g. surfactant, polymer), the composition and size of the NPs as well as the aqueous solution used [42]. It is possible to formulate NP using different surfactants changing their surface characteristics [43,44] or different polymers [43,45]. The nano-emulsion templating method also allows the control of the NP size by changing the ionic strength [42]. Moreover, this method presents a high capacity to encapsulate active agents with hydrophobic drug encapsulation percentages above 98% [43,46] and it can be used to encapsulate markers such as fluorophores[47] or metallic NPs [48,49]. Once nanoparticles are formed, their surface can be modified by different procedures, such as covalent binding or electrostatic interaction, and the molecule of interest (peptides, antibodies, dendrons, DNA…) incorporated on the surface [50–54].

In this work six different types of polymeric NPs, representative for some of the most used formulations in biomedical applications, were synthesized and studied: 1) PLGA NPs, 2) PLGA NPs containing a fluorophore (rhodamine 6 G) in the inner core, 3) PLGA NPs functionalized with antibodies, 4) PLGA NPs functionalized with dendrons, 5) ethyl cellulose (EC) NPs and 6) EC NPs prepared with a cationic surfactant. Using them a multiparametric nanomechanical analysis involving the Young's modulus, the breakthrough force, and the maximum sustained indentation has been performed at the single NP level by means of AFM force spectroscopy. The multiparametric study covers from small elastic deformations to large deformations and finally the NPs' rupture, thus containing all relevant mechanical information.

Results demonstrate that both surface functionalization and loading can strongly affect the overall mechanical properties of polymeric NPs, and hence, they can also affect the NPs stability, their circulation time, internalization efficiency, etc. Therefore, the nanomechanical dimension related to the introduction of surface functionalization and loading in polymeric NPs should be carefully considered in the design and production of efficient drug carriers.

2. Material and methods

2.1. Materials

Pharmaceutical grade Poly (lactic-co-glycolic acid), Resomer 752 H (PLGA) (polystyrene equivalent molecular weight PSE – MW~10,000 g/mol, determined by Gel Permeation Chromathography, was acquired from Evonik. The PLGA lactic to glycolic acid ratio was 75/25 and the end groups were free-carboxylic acids. Ethylcellulose, was from Colorcon (ETHOCEL™ Premium Std 10 ethylcellulose polymer). Ethoxyl content was 48.7% and the weight-average molecular weight (Mw) was 66385 ± 322 Da with a polydispersity of 4.3 as determined by Gel Permeation Chromatography[45]. Ethyl acetate and ethanol were used as the organic volatile solvents and purchased from Merck. Polysorbate 80 was kindly provided by Croda. The cationic amphiphile (CatA), ricinoleamidopropyltrimonium methosulfate was from Evonik. Kolliphor EL (also known as Cremophor®EL, CEL), a nonionic surfactant, was acquired from BASF. Water was MilliQ filtered (Millipore). Salts used to prepare the phosphate buffered saline (PBS, 0.16 M, pH = 7.4, 300 mOsm/kg) were sodium chloride, Disodium monohydrogenphosphate dihydrate and Sodium dihydrogenphosphate monohydrate, purchased from Merck. HEPES salt (4-(2-Hydroxyethyl)piperazine-1-ethanesulfonic acid) was from Sigma Aldrich. Rhodamine 6 G (Rho6G) was purchased at Sigma-Adrich. The 8D3 mouse monoclonal antibody against the transferrin receptor (8D3) was obtained from Bionova (MW = 160 kDa). N-(3-dimethylaminopropyl)-N-ethylcarbodiimide hydrochloride (EDC) was purchased from Fluka and N-hydroxisuccinimide sodium salt (NHS) from Sigma-Aldrich. Third generation Cationic dendrons with a primary amine focal point, a carbosilane structure and a quaternary amine with a positive charge at each ramification were kindly provided by Rafael Gomez group, from Universidad de Alcalá (Spain).

2.2. Formulation and preparation of nanoparticles

Six different types of nanoparticles (NP) were prepared for this study: PLGA nanoparticles (PLGA-NP), PLGA-NP containing Rhodamine 6 G (PLGA-Rho), PLGA NP functionalized with dendrons (PLGA-dendron), PLGA NP functionalized with 8D3 antibodies (PLGA-Ab), ethyl cellulose nanoparticles (EC-NP) and ethyl cellulose NP prepared using a cationic surfactant (EC-cationic).

All nanoparticles were prepared with the same approach, the nano-emulsion templating using the phase inversion composition (PIC) emulsification method to obtain nano-emulsions [40,43]. In brief, to create nano-emulsions the aqueous solution was stepwise added over an oil/surfactant (O/S) mixture (containing the polymer) at room temperature under continuous vortexing. The nanoparticle dispersions were prepared from the nano-emulsions by evaporating the solvent under reduced pressure using a Büchi R-215 V Rotavapor (for 4 g of nano-emulsion: 43mbar, 25ºC, 150 rpm). After that, the volume was adjusted with Milli-Q water to maintain the osmolality of the sample around 300 mOsm/kg.

2.2.1. PLGA NP

PLGA nanoparticles were prepared using a nano-emulsion formulation optimized elsewhere [43], PBS 0.16 M as aqueous solution (90% wt), Polysorbate as surfactant and ethyl acetate containing 4%wt of PLGA as oil. The used O/S ratio was 70/30.

Same components and composition than PLGA NP were used for PLGA-Rho NP except for the organic solvent that was changed by a mixture of ethyl acetate and ethanol (80/20) containing 0.1% wt of Rho6G [47].

2.2.2. Surface functionalization

Already prepared PLGA NP were functionalized with two different molecules, dendrons and antibodies, to obtain two new types of NP, PLGA-dendron and PLGA-Ab respectively. In both cases the PLGA NP surface was functionalized by means of covalent attachment between the carboxylic groups of PLGA polymer and the amines of dendrons or the antibodies. The procedure used, the carbodiimide reaction, was described elsewhere, [55] and [43], for dendrons and antibodies respectively.

Briefly, PLGA NPs were acidified with HCl 1 M (pH 5.5). An excess of EDC and NHS was added to nanoparticles, and the mixture was stirred for around 2 h at 25 ºC. After this time, activated nanoparticle dispersion was basified using NaOH 1 M (pH 8), as well as a solution of the dendron or 8D3 anti-transferrin receptor monoclonal antibody at the required molar ratio. Components were mixed and stirred for at least 18 h, at room temperature (25 ºC) to achieve their covalent binding. Finally, the functionalized nanoparticles were purified to remove the remaining reactants using a dialysis bag with a MWCO = 10,000–15,000 for 3 h in 2 L of water followed by three more hours in 250 mL of Hepes buffer 20 mM.

This procedure was demonstrated not to affect the antibody structure and functionality. Nanoparticles were not affected by these slight pH changes. The antibody and dendron covalent attachment were assessed previously [43,55].

2.2.3. Ethyl cellulose NP

Ethyl cellulose NP (EC) were prepared using Hepes 20 mM (95% wt of the final nano-emulsion), ethyl cellulose 6% wt in ethyl acetate and Polysorbate (for EC) or a mixture 1:1 of CatA:CEL (for EC-cationic) as surfactant [54].

2.3. Nano-emulsion and nanoparticle characterization

The quality and physicochemical properties of the template nano-emulsions and most of the resulting nanoparticles were evaluated previously [43,46,50,56]. Even so, visual assessment and dynamic light scattering measurements were routinely performed to assure the quality of the samples used in this study. The mean droplet size of nano-emulsions and the nanoparticle dispersions were measured by dynamic light scattering (DLS) with the 3D LS Spectrometer by LS Instruments (3D cross correlation multiple-scattering) equipped with a He–Ne laser (632.8 nm) with variable intensity. Measurements were carried out at a scattering angle of 90°, in triplicates, at 25 °C. Data were treated by cumulant analysis. The results are given as mean hydrodynamic sizes with the standard deviation of the populations considering the Polydispersity index. DLS measurements were performed at the ICTS NANBIOSIS by the Nanostructured Liquids Unit (U12) of the CIBER in Bioengineering, Biomaterials & Nanomedicine (CIBER-BBN), located at the IQAC-CSIC.

2.4. Atomic Force Microscopy (AFM) imaging and force spectroscopy measurements

2.4.1. Sample deposition

The ionic strength and the aqueous solution used during the preparation of the nano-emulsion it is known to affect the size of the nanoparticles prepared by nano-emulsion templating [42]. But once the NPs are formed their size is not substantially affected by changes in the aqueous solution. On the other hand the ionic strength can affect the AFM image quality due to non-balanced electrostatically charges [57]. For this reason, and to homogenize the measuring conditions, NP were prepared using the aqueous solutions mentioned above, but subsequently dialyzed and its aqueous solution changed to Hepes 20 mM pH 7.4.

100 μL of NP dispersion were deposited on freshly cleaved high-quality mica and incubated for 15 min. For anionic NP 10 μL of $CaCl_2$ 10 mM solution was added prior NP deposition to enhance the NPs adherence to mica. After incubation samples were rinsed with Hepes 20 mM pH7.4. *Imaging conditions:* Topographic images and force–distance curves were acquired in Hepes solution with a Nanotec Electronica AFM using Pyrex silicon nitride tips PNP-DB (Nanoworld) with a nominal spring constant of 0.06 N/m, resonance frequency in liquid of ~19 kHz, pyramidal apex, and a typical tip radius < 10 nm. All measurements were performed in a closed chamber with humid air to avoid evaporation of the Hepes solution. Tips were prewet with 20 μL of buffer to avoid tip damage due to surface tension during the approach.

Topography images were obtained in intermittent contact dynamic mode. In this image mode the cantilever is oscillated close to its resonance frequency and renders intermittent contact between the tip and the sample reducing the potential damage due to frictional forces compared with contact mode.

2.4.2. Force spectroscopy

Force spectroscopy measurements were performed on isolated nanoparticles. For force spectroscopy measurements the scanning area was first limited to individual NPs and then the scanning was stopped in the line corresponding to the central region of the NP. Force distance (Fz) curves were measured at the center of the scanning line and the topography profile monitored continuously including before and after the Fz's. Curves were extended a fixed range of 200–300 nm. To assess the presence of eventual viscoelastic effects, plastic deformations or slow shape recoveries measurements at different tip approach speeds and at different rates between consecutive force curves have been performed.

2.4.3. Software and analysis

WSxM software was used for the processing of images and force curves [58]. WSxM flooding tool was used to measure the area, perimeter, z max and volume of the NPs from the images obtained and used to calculate the estimated size. Young's modulus was extracted using AtomicJ, by using Hertz model and a paraboloid tip geometry [59] and considering the first 5–10 nm after contact. Breakthrough force, Young's

modulus, adhesion and total indentation values correspond to mean values ± standard deviation of at least 30 Fz's obtained in different NPs and different experiments (N ≥ 3).

2.5. Statistics

Statistical analysis was performed using OriginPro. Data are represented as mean ± standard deviation. Statistical significance was determined by One-way ANOVA followed by Tukey method. $p < 0.05$ was considered statistically significant. Representations of Tukey analysis are included in Supplementary information.

3. Results and discussion

Polymeric Nanoparticles were prepared by nano-emulsion templating using nano-emulsions previously prepared by the Phase Inversion Composition (PIC) method (Fig. 1a) [40,41,60].

The PIC is a low-energy emulsifying method that uses the intrinsic chemical energy of the system for the formation of nano-emulsions by a change in the spontaneous curvature of the surfactant as consequence of a gradual change in the composition during preparation at constant temperature [40,41,60] (a schematic representation is shown in Fig. 1a). As it can be performed at mild conditions and allows obtaining polymeric nano-emulsions using preformed polymers, this emulsification

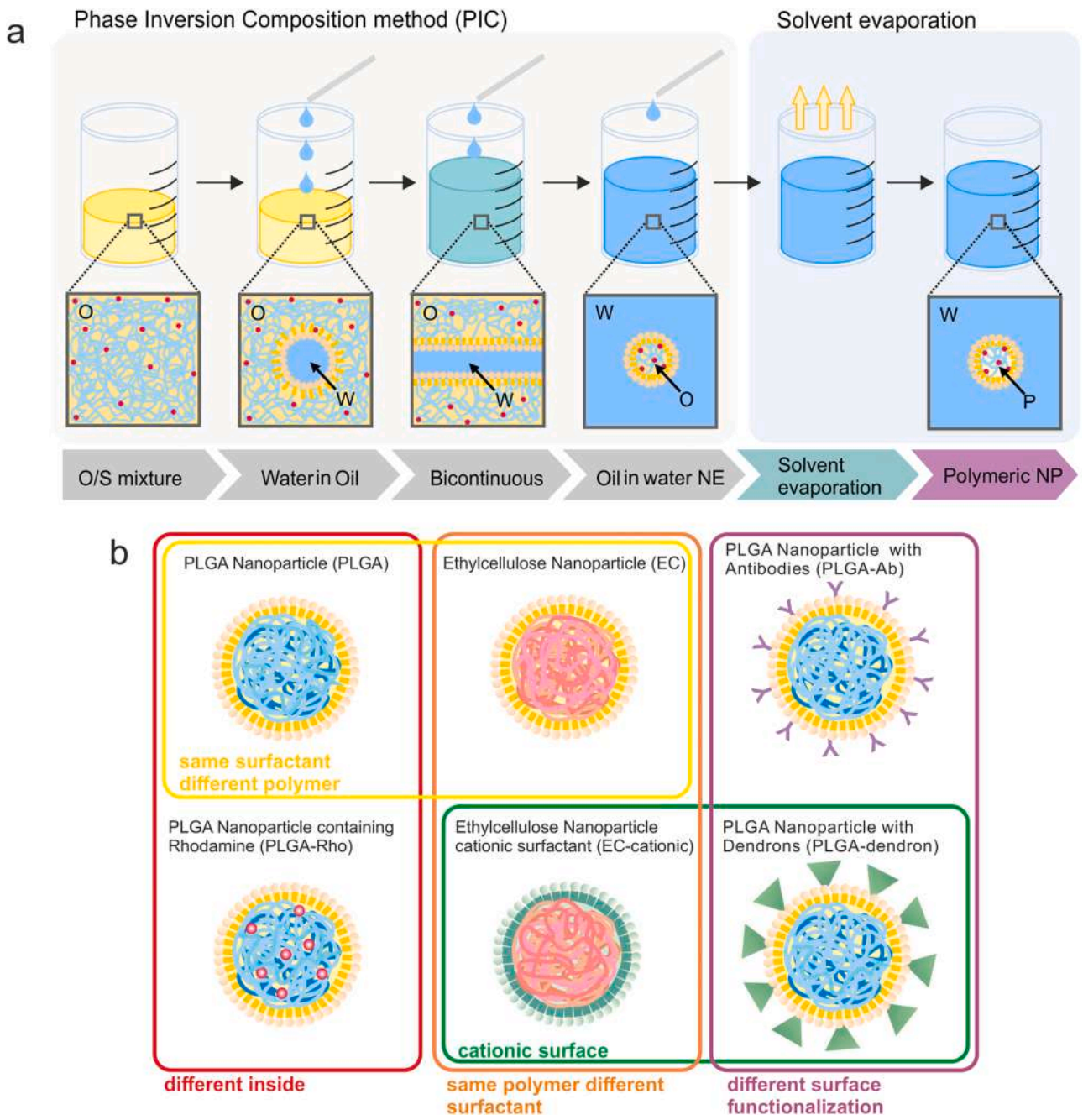

Fig. 1. Polymeric Nanoparticles from Nano-emulsion templating. (a) Schematic representation of Preparation of polymeric Nanoparticles by Nano-emulsion templating. O: oil (contains solvent, polymer and molecules to be encapsulated), S: surfactant, W: aqueous solution, P: polymer. (b) Schematic representation of the studied PLGA Nanoparticles (PLGA), Ethyl cellulose Nanoparticles (EC), PLGA Nanoparticles functionalized with antibodies (PLGA-Ab), PLGA Nanoparticles containing Rhodamine 6 G (PLGA-Rho), Ethyl cellulose Nanoparticles with cationic surfactant (EC-cationic) and PLGA nanoparticles with dendrons (PLGA-dendron).

method is relevant to entrap labile components for health, pharmaceutic, cosmetic and detergency industries, resulting in formulations without traces of monomers, frequently present with in situ polymerization strategies [41,56]. The later removal of the organic solvent from the nano-emulsion gives rise to a nanoparticle dispersion (Fig. 1a).

In the present study, six different types of polymeric Nanoparticles were prepared and characterized following this method (Fig. 1b): PLGA NP (PLGA), ethyl cellulose NP (EC), ethyl cellulose NP with a cationic surfactant (EC-Cationic), PLGA NP with encapsulated Rhodamine (PLGA-Rho), PLGA NP coated with dendrons (PLGA-Dendron) and PLGA

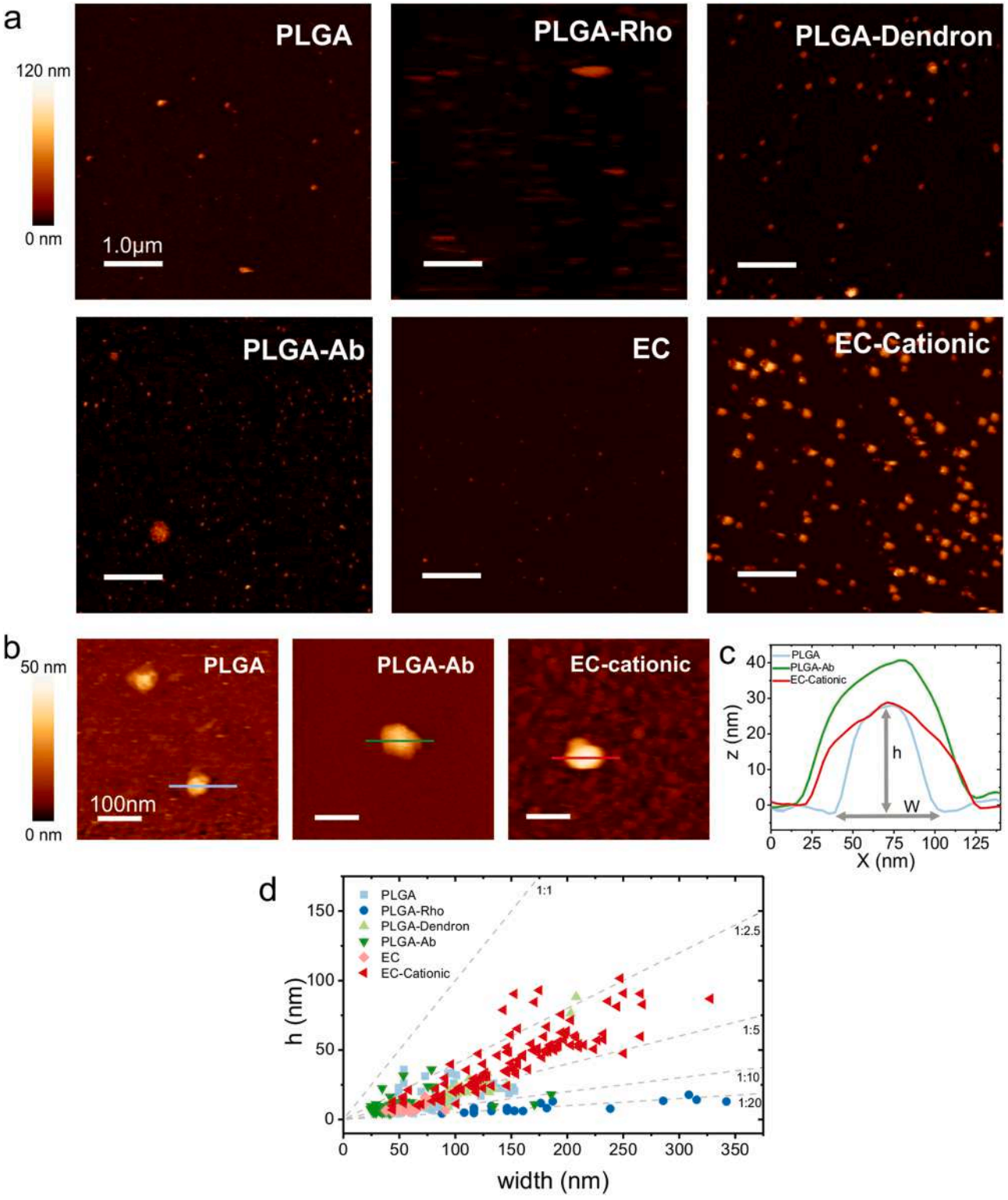

Fig. 2. AFM imaging of Polymeric Nanoparticles. (a) AFM topography images of PLGA, PLGA-Rho, PLGA-Dendron, PLGA-Ab, EC and EC-cationic. (b) Representative topography images of individual NP of PLGA, PLGA-Ab and EC-cationic. (c) Profiles corresponding to NPs cross-sections along the lines in Fig. B: PLGA light blue, PLGA-Ab green and EC-cationic red. (d) Height, *h*, versus width, *W*, of the NPs absorbed on mica substrate estimated from topographic images. Dashed grey lines indicate different *h:W* aspect ratios.

NP coated with antibodies (PLGA-Ab). These NPs constitute examples of gold-standard functionalizations in drug delivery systems and allow comparing individually different factors as the effect of polymer, surfactant, surface functionalization, cationic surface or presence of entrapped molecules (Fig. 1b).

The studied polymeric nanoparticle dispersions have demonstrated their efficacy in vitro or in vivo and present hydrodynamic radii in the range of tens of nanometers [43,45,47,50,54,61]. For the present study, PLGA NPs presented a hydrodynamic radius of 27 ± 9 nm, PLGA-Rho 38 ± 21 nm, PLGA-Dendron 29 ± 13 nm, PLGA-Ab 32 ± 21 nm, EC NPs 83 ± 41 nm and EC-cationic 39 ± 25 nm.

3.1. AFM imaging of polymeric nanoparticles

Nanoparticles were characterized by Atomic Force Microscopy (AFM). Fig. 2a shows representative topographic AFM images obtained on the different NPs considered. Images were obtained in Hepes buffer in intermittent contact dynamic mode [62,63]. In all AFM images, structures with sizes and shape compatible with the NPs were observed. Surface coverage was clearly dependent on the NP type due to the differences in NP surface properties and their interaction with the mica substrate. As expected, cationic NPs (PLGA-Dendron and EC-cationic) presented a greater adsorption to the negatively charged mica than anionic NPs leading to an increased coverage of the substrate surface. PLGA-Rho NPs presented difficulties to be imaged, resulting on images of poor definition and elongated NP shape. These difficulties were a consequence of the weak interaction of PLGA-Rho NPs with the mica substrate. However, this weak immobilization did not affect force spectroscopy measurements, in which the tip performs a purely vertical motion.

Fig. 2b-c show representative examples of AFM topography images of single NPs and their topographic profiles. As can be observed, NPs showed a width (W) greater than its height (h). This effect can be better recognized in Fig. 2d, where the height versus width is represented for the different populations of analysed NPs. The grey dashed lines represent different height:width aspect ratios. In all cases, aspect-ratio was below 1 (1:1, height: width) that would correspond to a spherical nanoparticle, being most of the NPs in the 1:2.5–1:10 range, and even 1:20 for PLGA-Rho. The flattening of soft nanoparticles and nanovesicles adsorbed on solid supports is a frequent observation. It is attributed to the combination of the slight pressure made by the tip during imaging (magnified by the small size of the tips used, <10 nm), the tip convolution and a small deformation of NPs during its adsorption to the mica surface due to its soft nature [64–66]. Even so, a good correlation between the hydrodynamic sizes and the equivalent radius extracted from AFM measurements was observed in most cases (see Fig. S1).

3.2. Mechanical properties of polymeric nanoparticles

NPs were mechanically characterized at the single nanoparticle level by individually puncturing them with the AFM tip probe and measuring the force acting on it from the cantilever bending and tip vertical displacement. Fig. 3a shows a characteristic plot of the force acting on the probe as a function of the tip indentation into the nanoparticle during approach (dark) and retract (light). From approach curves we can extract different quantitative mechanical parameters, indicators of different properties: 1) the Young's modulus, 2) the rupture point corresponding to the breakthrough force and 3) the maximum indentation. The Young's modulus is a standard parameter used to quantify the elasticity of a material in response to small deformations. The breakthrough force represents the maximum force a material is able to withstand before its rupture. Finally, the total indentation is the distance from the initial tip-nanoparticle interaction to the final tip-substrate interaction and provides evidence of the maximum deformability a NP can sustain before its rupture. In addition, the adhesion force, necessary to detach the tip from the nanoparticle, can be determined from the

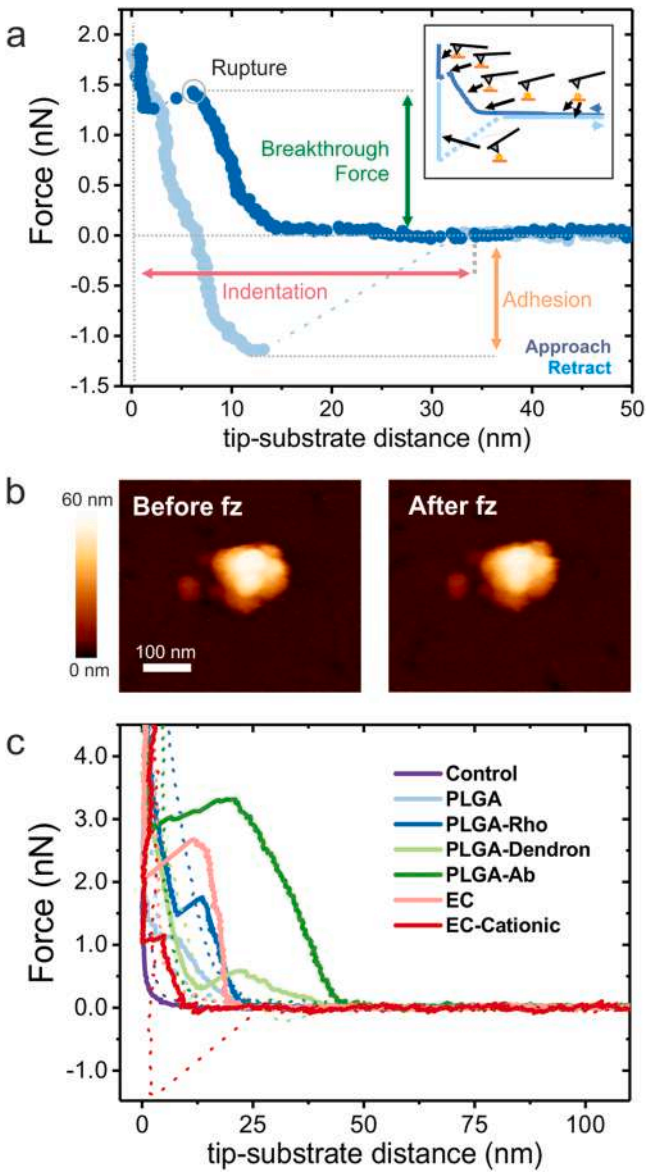

Fig. 3. Force spectroscopy of polymeric nanoparticles. (a) Force vs tip-substrate distance representation indicating important parameters: Rupture, Breakthrough Force, Indentation and Adhesion. Inset: Schematic representation of forward and backward Force vs tip-substrate distance curves and the corresponding configuration of the AFM tip-NP. (b) AFM topography image of EC-cationic NP before and after a fz. (c) Representative Force vs Tip-substrate distance curves as a function of NP functionalization (forward-solid line, backward-dotted line).

retraction curve (light blue symbols in Fig. 3a). The presence the breakthrough events are displayed by horizontal discontinuities in the Fz curves, the adhesion by negative peaks in the withdraw curve, while the tip to mica contact corresponds to the point in which the Fz becomes a vertical line (Fig. 3a).

Fz experimental conditions were optimized to minimize the viscous effects, plastic deformations, aging or slow elastic recovery effects (more information about the optimization process on Supporting Information S2). The integrity of the NPs indentation was also evaluated by imaging the NPs before and after the individual Fz's (see an example corresponding to an EC-Cationic NP in Fig. 3b). This test was routinely performed for all the measured samples. Despite the fact that NPs were punctured until a break event was observed and the tip-mica contact detected, none of the NPs considered in this study showed permanent

rupture or deformation in the topography images under the measuring conditions used. This result suggests the presence of a self-healing phenomenon, like the observed on membranes, liposomes or other similar nanovesicles. This self-healing behavior is suspected to be a consequence of the structure of the NPs prepared by nano-emulsion templating. By this procedure NPs have the structure of the former nano-emulsion droplet, containing the preformed polymer in the core (PLGA or ethyl cellulose in our case) surrounded by a layer of surfactant acting as a barrier of the droplet or NP [40,41]. It is described in literature that two effects are observed in self-healing materials, 1) a mobility or flow of a mobile phase and 2) a rebuilt of the polymer network to restore the mechanical integrity of the system [67,68]. In our NPs, apart from the flexibility and the capability to rearrange of the preformed polymer itself, we hypothesize the surfactant layer to be responsible of the self-healing character of our NPs acting as mobile phase due to their self-assembling character. For other experimental conditions, e.g. higher speeds or consecutive Fzs with short time between them, the self-healing character can be altered due to the lack of enough time for recovery (see Fig. S2.5).

Fig. 3c shows representative examples of single Fz curves taken on mica surface (control) and the different NPs studied (PLGA, PLGA-Rho, PLGA-dendron, PLGA-Ab, EC and EC-cationic). From these

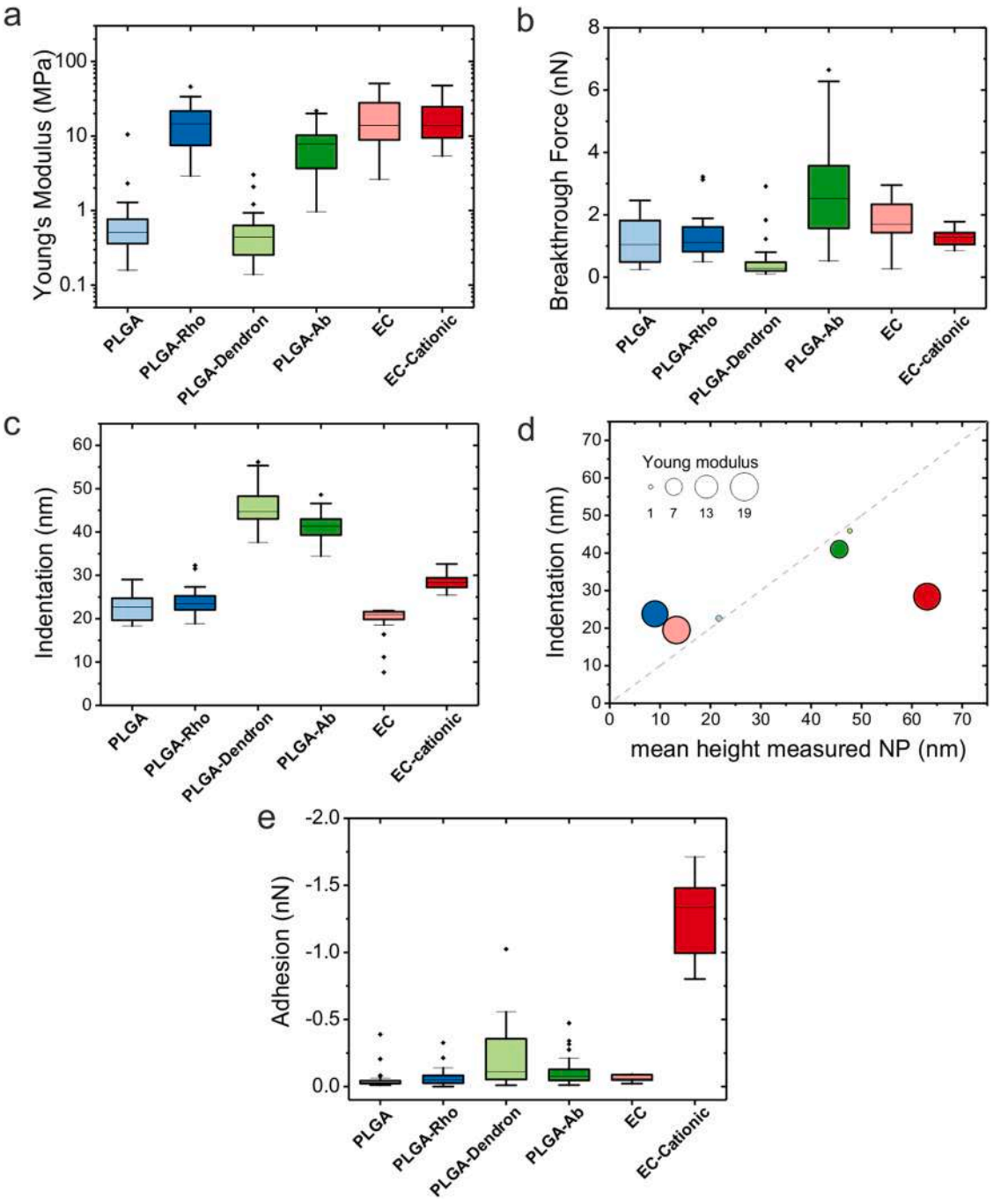

Fig. 4. Mechanics of polymeric nanoparticles depending on their functionalization. (a) Young's modulus (MPa) (b) Breakthrough Forces (nN) (c) Indentation (nm) and (e) Adhesion (nN) for the different nanoparticles evaluated. (d) Indentation (nm) vs mean height of the measured NP (nm) and represented as a function of their Young's Modulus (MPa). Horizontal line indicates median values. Dotted line indicates ratio 1:1. Fig. S3.1–4 contain the Plot of Tukey analysis about the statistical significant difference of the populations.

representative Fz's it is possible to already observe differences between the different types of NPs, which are analyzed on what follows.

The quantitative parameters that define NP mechanical resistance were extracted from the Fz. Fig. 4 shows the Young's modulus, breakthrough force, maximum indentation after rupture and adhesion force extracted from the Fz obtained for each type of NP.

The Young's moduli of the studied NPs (Fig. 4a) were obtained using the Hertz model assuming a paraboloid geometry and following the methodology previously used in other soft nanoparticles [69,70]. The model used considers the approach curves for the analysis and assumed a Poisson's ratio of 0.25 [71], small indentations (5–10 nm) and a tip radius of 10 nm. The resulting Young's moduli showed values in the kPa-MPa range, in accordance with previous results in literature for polymeric NPs [72]. Tukey analysis on the difference between the analyzed populations is represented in Fig. S3.1. The lowest Young's moduli correspond to PLGA and PLGA-dendron NPs, 0.95 ± 2 MPa and 0.6 ± 0.6 MPa, respectively, while highest correspond to ethyl cellulose NPs,19 ± 13 MPa and 18 ± 11 MPa for EC and EC-cationic respectively. Interestingly, the PLGA-Rho and PLGA-Ab NPs presented Young's modulus values closer to the values of EC NPs, 17 ± 10 MPa and 8 ± 5 MPa, respectively, which are much higher than those obtained for bare PLGA NPs. Therefore, the loading of PLGA NPs with Rho6G or the surface functionalization with Ab ended up in NPs with a Young's modulus significantly different from the naked PLGA NPs. At the same time the use of different surfactant (in case of EC NPs) or the incorporation of dendrons (for PLGA NPs) does not imply a significative difference. Since the composition and preparation of PLGA and PLGA-Rho NPs are similar, the presence of Rhodamine 6 G (Rho6G) at the inner core is considered the responsible for the increment of the Young's modulus of these NPs. Rho6G molecules are entrapped between the PLGA at the polymeric core of the NPs. The efficiency of encapsulation of the fluorophore is higher than the 99% (ref) and taking into account the quantity of Rho6G used in the formulation it corresponds to a weight and molar ratio (Rho6G/ PLGA) of 1:40 and 1:2 respectively. Rho6G is a cationic molecule while PLGA is anionic. We hypothesize the presence of this small molecules at the inner core of the NPs could be acting similarly to cross-linkers, but by means of hydrophobic and electrostatic interaction instead of covalent bonding. Thus, Rho6G would interact with PLGA molecules reducing their mobility and increasing the resulting Young's modulus. For PLGA NPs with antibodies on their surface (PLGA-Ab), their Young's modulus agrees with the range of the previously described values for antibodies, i.e. 2.5–9 MPa depending on the force loading [73]. For EC-Cationic NPs, the presence of different surfactant and charges at their surface did not imply a significant difference in the Young's modulus compared with bare EC NPs (Fig. 4a and Fig. S3.1). Focusing on the used polymer (EC or PLGA) has a strong effect in the Young modulus, with bare EC showing notably higher values (see above).

Regarding the breakthrough forces, the maximum force the NP withstands before its rupture, a different trend is observed (Fig. 4b). In this case, all NPs presented similar values, in the range of 0–3nN, except PLGA-Ab that presented significantly higher mean values and with higher dispersion, 2.17 ± 1.5 nN (Fig. 4b and Fig. S3.2). It is worth mentioning that in case of using the carbodiimide reaction for the functionalization with antibodies, as in this study, the antibody binding is not directed, resulting in differently oriented moieties and different homogeneity of coverage. Thus, the concentration of antibodies and orientation of the antibody could be different from NP to NP and, as consequence, being one of the reasons for the higher dispersion in the measured breakthrough forces.

Fig. 4c shows the quantified values for the total indentation, this is the indentation achieved until the contact with the substrate after the breakthrough is detected. These indentation values do not correspond to those used to determine the Young's modulus which were limited only to the range 5–10 nm. As expected, NPs with functionalized surfaces presented higher total indentation values, 46 ± 55 nm and 41 ± 3 nm for PLGA-dendron and PLGA-Ab NPs, respectively. NPs with *naked* surfaces (PLGA, PLGA-Rho, EC and EC-cationic) presented similar values even with different polymer and surfactant, 22 ± 3 nm, 24 ± 3 nm, 19 ± 4 nm and 28 ± 2 nm. Previous studies on colloidal polymer droplets suggested that at intermediate levels of cross-linking the polymer droplet deformability depends on two factors, the rheology of the droplet and the interfacial tension, but at low levels of cross-linking it is mainly affected by the interfacial tension.[74] Our indentation results, obtained on NPs with preformed polymer and showing differences as a function of the type of coating used, suggest a similar effect and a dependence with interfacial forces. Complementary information is given in Fig. 4d where the maximum indentation as a function of the mean height of the NPs measured is represented. In the plot the symbols are proportional to the value of Young's modulus (see also Fig. S4). We observe that PLGA, PLGA-Dendron, PLGA-Ab and EC NPs are close to the ideal, height: indentation 1:1 ratio, being the populations with the lowest Young's modulus the ones closest to the ideal ratio. It is worth mention that even the ratio between them is close to the ideal one (Fig. 4d) there are variability in the measurements and small discrepancies between height and indentation due to experimental conditions (setpoint used, pixel size…). This is evidenced in Fig. S4 where it is possible to observe that topography measurements have a greater dispersion than force spectroscopy measurements. In case of PLGA-Rho the obtained ratio showed a lower height compared with indentation. This result is in accordance with the topography measurements as PLGA-Rho showed difficulties to be imaged but no difficulties during force spectroscopy measurements. In the case of EC-Cationic the behavior is different, the height represented in the topographic AFM images is higher than the values obtained for the indentation. This may indicate that these NPs compress in such a way that the NPs are not completely pierced during the indentation of the AFM probe in the range of forces used.

Concerning adhesion force values (Fig. 4e), all NPs presented values close to zero except cationic NPs (PLGA-dendron and EC-cationic), which presented higher values (see analysis of the significative difference on Fig. S3.4). Thus, the addition of cationic charge results in an increment of the AFM tip-NP interaction and an increment of the adhesion values. These results suggest that, as could be expected, surface charge is more relevant in adhesion than in other parameters. It is worth mentioning that these higher adhesions are observed under specific experimental conditions and in vivo this behavior could be altered by the presence of the protein corona that at the same time is known to be affected by the size and surface characteristics of the NPs[75,76].

The results obtained suggest that the role of surface functionalization and/or loading on the mechanical properties of NPs does not follow a simple trend. Table 1 summarizes the effects of the different factors analyzed in the present work on the different mechanical parameters and in the adhesion. These results show that the overall mechanical properties of polymer NPs can be affected in several different ways depending on the functionalization or loading performed, further evidencing the importance of performing a multiparametric mechanical analysis, as the one reported here, for every particular type of NP.

Given the different aspects addressed by the different mechanical factors measured, the overall mechanical properties of the nanoparticles can be assessed through a cluster graph build from the three different mechanical properties measured (Young's modulus, indentation and breakthrough force) for the different NPs. Fig. 5 shows this representation for the NPs analyzed in the present work (Fig. S5 shows the corresponding projections in the 2D planes). The graph provides information on the elastic response to small deformations (Young's modulus), the maximum deformability attainable (Indentation) and the maximum force that a given nanoparticle type can sustain (Breakthrough force). Nanoparticles clustering together present similar overall mechanical properties, while those clustering apart display distinct mechanical properties in one or more aspects. In the present study, we observe 4 differentiated groups. PLGA-Rho, EC and EC-cationic NPs

Table 1
Effect of composition, loading and functionalization on the mechanics of NPs.

Characteristics studied	Reference NP	NP	Young's modulus	Breakthrough Force	Indentation	Adhesion
Different polymer/ same surfactant	PLGA	EC	≠	=	≠	=
Different loading/ same surface and polymer	PLGA	PLGA-Rho	≠	=	=	=
Different surface (Ab)/ same polymer	PLGA	PLGA-Ab	≠	≠	≠	=
Different surface (cationic dendron)/ same polymer	PLGA	PLGA-Dendron	=	=	≠	≠
Different surfactant (cationic)/same polymer	EC	EC-Cationic	=	=	=	≠

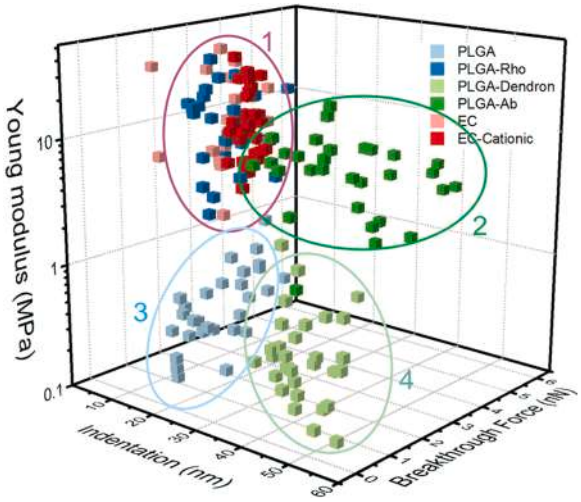

Fig. 5. Multiparametric mechanical 3D representation. X Breakthrough Force (nN), Y Indentation (nm) and Z Young's modulus (MPa) for the different nanoparticles evaluated.

display similar mechanical properties (group 1 in Fig. 5), while PLGA, PLGA-Ab and PLGA-dendron show distinct overall mechanical properties (groups 3, 2 and 4 in Fig. 5 respectively). Adhesion would help as a complementary information to unravel similar populations. Given the relevance of the mechanical properties of polymeric NPs in cell uptake and body distribution, it could be expected that NPs displaying different overall mechanical properties would also show different cell uptake and distributions (although of course other factors should be also considered, as mentioned before). Therefore, the realization of multiparametric nanomechanical characterizations and of multidimensional mechanical plots can be of major use in the analysis of the nanomechanical properties of different polymeric NPs formulations.

4. Conclusions

The mechanical properties of six different types of NPs with different surface functionalization or loadings (namely, PLGA, PLGA-Rho, PLGA-dendron, PLGA-Ab, EC and EC-cationic) and used as delivery system in biomedical application, have been evaluated by Atomic Force Microscopy force spectroscopy. Values of Young's modulus, breakthrough force, total indentation and adhesion force were obtained for each type of nanoparticles and showed a non-trivial dependence on the surface functionalization or loading, demonstrating that the overall mechanical properties of polymer NPs constitute a complex and multifactorial problem. In reaching these results, it has been key the use of the Nanoemulsion templating approach using the low-energy Phase Inversion Composition method (PIC) to obtain the nano-emulsion. This process possesses the appropriate versatility to create NPs of similar sizes with different polymers, and surfactants, incorporating a fluorophore at the inner core or attaching surface functionalization. A graphical representation has been proposed to facilitate the identification of NPs with similar overall mechanical properties, which can be useful in the mechanical optimization of drug polymer nanocarriers. Our results demonstrate that since NPs mechanics can be altered by its surface functionalization or loading, nanomechanical analysis of NPs should be considered in general in the process of designing and formulating NPs with optimized and enhanced cell uptake or bioavailability. These results evidence the need to carefully consider these properties before their preclinical and clinical use in addition to the commonly studied non-mechanical parameters such as the stability of the preparation or its binding efficiency.

CRediT authorship contribution statement

Aurora Dols-Perez: Conceptualization, Methodology, Investigation, Writing – original draft, Visualization. **Cristina Fornaguera:** Investigation, Methodology, Writing – original draft. **Natalia Feiner-Gracia:** Investigation, Writing – review & editing. **Santiago Grijalvo:** Investigation, Writing – review & editing. **Conxita Solans:** Supervision, Writing – original draft, Funding acquisition. **Gabriel Gomila:** Supervision, Writing – original draft, Funding acquisition.

Declaration of Competing Interest

The authors declare that they have no known competing financial interests or personal relationships that could have appeared to influence the work reported in this paper.

Data availability

The datasets used and/or analyzed during the current study are available from the corresponding author on reasonable request.

Acknowledgments

CIBER-BBN is an initiative funded by the Spanish National Plan for Scientific and Technical Research and Innovation 2013–2016, Iniciativa Ingenio 2010, Consolider Program, CIBER Actions are financed by the Instituto de Salud Carlos III with assistance from the European Regional Development Fund. A.D-P. has received funding from the postdoctoral fellowships program Beatriu de Pinós, funded by the Secretary of Universities and Research (Government of Catalonia) and by the Horizon 2020 program of research and innovation of the European Union under the Marie Skłodowska-Curie grant agreement No. 801370. G.G and A.D-P acknowledges support from MINECO/FEDER (grant PID2019–110210GB-I00). C.F.P. Acknowledges the support from MINECO/FEDER (grant RTI2018–094734-B-C22). Rafael Gomez group is acknowledged for the dendron cession.

Appendix A. Supporting information

Supplementary data associated with this article can be found in the online version at doi:10.1016/j.colsurfb.2022.113019.

References

[1] C. Fornaguera, J.M. García-Celma, Personalized nanomedicine: a revolution at the nanoscale, J. Pers. Med. 7 (4) (2017).

[2] J. Pan, K. Rostamizadeh, N. Filipczak, V.P. Torchilin, Polymeric co-delivery systems in cancer treatment: an overview on component drugs' dosage ratio effect, Molecules 24 (6) (2019) 1035.
[3] E. Fattal, H. Hillaireau, S. Mura, J. Nicolas, N. Tsapis, Targeted delivery using biodegradable polymeric nanoparticles, in: J. Siepmann, R.A. Siegel, M. J. Rathbone (Eds.), Fundamentals and Applications of Controlled Release Drug Delivery, Springer US, Boston, MA, 2012, pp. 255–288.
[4] S. Mitragotri, J. Lahann, Physical approaches to biomaterial design, Nat. Mater. 8 (1) (2009) 15–23.
[5] L. Gong, K. He, J. Liu, Concentration-dependent subcellular distribution of ultrasmall near-infrared-emitting gold nanoparticles, Angew. Chem. Int. Ed. 60 (11) (2021) 5739–5743.
[6] H. Cabral, Y. Matsumoto, K. Mizuno, Q. Chen, M. Murakami, M. Kimura, Y. Terada, M.R. Kano, K. Miyazono, M. Uesaka, N. Nishiyama, K. Kataoka, Accumulation of sub-100 nm polymeric micelles in poorly permeable tumours depends on size, Nat. Nanotechnol. 6 (12) (2011) 815–823.
[7] H. Kang, S. Rho, W.R. Stiles, S. Hu, Y. Baek, D.W. Hwang, S. Kashiwagi, M.S. Kim, H.S. Choi, Size-Dependent EPR Effect of Polymeric Nanoparticles on Tumor Targeting, Adv. Health Mater. 9 (1) (2020), 1901223.
[8] J. Rejman, V. Oberle, I.S. Zuhorn, D. Hoekstra, Size-dependent internalization of particles via the pathways of clathrin- and caveolae-mediated endocytosis, Biochem J. 377 (Pt 1) (2004) 159–169.
[9] W. Jiang, B.Y.S. Kim, J.T. Rutka, W.C.W. Chan, Nanoparticle-mediated cellular response is size-dependent, Nat. Nanotechnol. 3 (3) (2008) 145–150.
[10] V. Torchilin, Tumor delivery of macromolecular drugs based on the EPR effect, Adv. Drug Deliv. Rev. 63 (3) (2011) 131–135.
[11] S. Schöttler, G. Becker, S. Winzen, T. Steinbach, K. Mohr, K. Landfester, V. Mailänder, F.R. Wurm, Protein adsorption is required for stealth effect of poly (ethylene glycol)- and poly(phosphoester)-coated nanocarriers, Nat. Nanotechnol. 11 (4) (2016) 372–377.
[12] N.M. La-Beck, A.A. Gabizon, Nanoparticle interactions with the immune system: clinical implications for liposome-based cancer chemotherapy, Front Immunol. 8 (2017), 416-416.
[13] B. Fadeel, Hide and seek: nanomaterial interactions with the immune system, Front Immunol. 10 (133) (2019).
[14] S. Barua, S. Mitragotri, Challenges associated with penetration of nanoparticles across cell and tissue barriers: a review of current status and future prospects, Nano Today 9 (2) (2014) 223–243.
[15] S. Behzadi, V. Serpooshan, W. Tao, M.A. Hamaly, M.Y. Alkawareek, E.C. Dreaden, D. Brown, A.M. Alkilany, O.C. Farokhzad, M. Mahmoudi, Cellular uptake of nanoparticles: journey inside the cell, Chem. Soc. Rev. 46 (14) (2017) 4218–4244.
[16] P. Foroozandeh, A.A. Aziz, Insight into cellular uptake and intracellular trafficking of nanoparticles, Nanoscale Res. Lett. 13 (1) (2018) 339.
[17] Y.-R. Zhang, R. Lin, H.-J. Li, W.-l He, J.-Z. Du, J. Wang, Strategies to improve tumor penetration of nanomedicines through nanoparticle design, WIREs Nanomed. Nanobiotechnology 11 (1) (2019), e1519.
[18] M. Nowak, T.D. Brown, A. Graham, M.E. Helgeson, S. Mitragotri, Size, shape, and flexibility influence nanoparticle transport across brain endothelium under flow, Bioeng. Transl. Med. 5 (2) (2020), e10153.
[19] J. Cui, R. De Rose, J.P. Best, A.P.R. Johnston, S. Alcantara, K. Liang, G.K. Such, S. J. Kent, F. Caruso, Mechanically Tunable, Self-Adjuvanting Nanoengineered Polypeptide Particles, Adv. Mater. 25 (25) (2013) 3468–3472.
[20] K.A. Beningo, Y.L. Wang, Fc-receptor-mediated phagocytosis is regulated by mechanical properties of the target, J. Cell Sci. 115 (Pt 4) (2002) 849–856.
[21] Y. Zheng, L. Xing, L. Chen, R. Zhou, J. Wu, X. Zhu, L. Li, Y. Xiang, R. Wu, L. Zhang, Y. Huang, Tailored elasticity combined with biomimetic surface promotes nanoparticle transcytosis to overcome mucosal epithelial barrier, Biomaterials 262 (2020), 120323.
[22] J. Chen, V. Kozlovskaya, A. Goins, J. Campos-Gomez, M. Saeed, E. Kharlampieva, Biocompatible Shaped Particles from Dried Multilayer Polymer Capsules, Biomacromolecules 14 (11) (2013) 3830–3841.
[23] L. Zhang, H. Chen, J. Xie, M. Becton, X. Wang, Interplay of Nanoparticle Rigidity and Its Translocation Ability through Cell Membrane, J. Phys. Chem. B 123 (42) (2019) 8923–8930.
[24] A.C. Anselmo, M. Zhang, S. Kumar, D.R. Vogus, S. Menegatti, M.E. Helgeson, S. Mitragotri, Elasticity of nanoparticles influences their blood circulation, phagocytosis, endocytosis, and targeting, ACS Nano 9 (3) (2015) 3169–3177.
[25] Y. Hui, D. Wibowo, Y. Liu, R. Ran, H.-F. Wang, A. Seth, A.P.J. Middelberg, C.-X. Zhao, Understanding the effects of nanocapsular mechanical property on passive and active tumor targeting, ACS Nano 12 (3) (2018) 2846–2857.
[26] L. Ribovski, E. de Jong, O. Mergel, G. Zu, D. Keskin, P. van Rijn, I.S. Zuhorn, Low nanogel stiffness favors nanogel transcytosis across an in vitro blood–brain barrier, Nanomed.: Nanotechnol., Biol. Med. 34 (2021), 102377.
[27] L. Zhang, Z. Cao, Y. Li, J.-R. Ella-Menye, T. Bai, S. Jiang, Softer zwitterionic nanogels for longer circulation and lower splenic accumulation, ACS Nano 6 (8) (2012) 6681–6686.
[28] J. Key, A.L. Palange, F. Gentile, S. Aryal, C. Stigliano, D. Di Mascolo, E. De Rosa, M. Cho, Y. Lee, J. Singh, P. Decuzzi, Soft discoidal polymeric nanoconstructs resist macrophage uptake and enhance vascular targeting in tumors, ACS Nano 9 (12) (2015) 11628–11641.
[29] M. Yu, L. Xu, F. Tian, Q. Su, N. Zheng, Y. Yang, J. Wang, A. Wang, C. Zhu, S. Guo, X. Zhang, Y. Gan, X. Shi, H. Gao, Rapid transport of deformation-tuned nanoparticles across biological hydrogels and cellular barriers, Nat. Commun. 9 (1) (2018) 2607.
[30] X. Chen, J. Cui, Y. Ping, T. Suma, F. Cavalieri, Q.A. Besford, G. Chen, J.A. Braunger, F. Caruso, Probing cell internalisation mechanics with polymer capsules, Nanoscale 8 (39) (2016) 17096–17101.
[31] R. Palankar, B.-E. Pinchasik, S. Schmidt, B.G. De Geest, A. Fery, H. Möhwald, A. G. Skirtach, M. Delcea, Mechanical strength and intracellular uptake of CaCO3-templated LbL capsules composed of biodegradable polyelectrolytes: the influence of the number of layers, J. Mater. Chem. B 1 (8) (2013) 1175–1181.
[32] J.K. Vasir, V. Labhasetwar, Quantification of the force of nanoparticle-cell membrane interactions and its influence on intracellular trafficking of nanoparticles, Biomaterials 29 (31) (2008) 4244–4252.
[33] N. Alsharif, B. Eshaghi, B.M. Reinhard, K.A. Brown, Physiologically relevant mechanics of biodegradable polyester nanoparticles, Nano Lett. 20 (10) (2020) 7536–7542.
[34] B.V. Slaughter, S.S. Khurshid, O.Z. Fisher, A. Khademhosseini, N.A. Peppas, Hydrogels in regenerative medicine, Adv. Mater. 21 (32–33) (2009) 3307–3329.
[35] X. Banquy, F. Suarez, A. Argaw, J.-M. Rabanel, P. Grutter, J.-F. Bouchard, P. Hildgen, S. Giasson, Effect of mechanical properties of hydrogel nanoparticles on macrophage cell uptake, Soft Matter 5 (20) (2009) 3984–3991.
[36] W. Liu, X. Zhou, Z. Mao, D. Yu, B. Wang, C. Gao, Uptake of hydrogel particles with different stiffness and its influence on HepG2 cell functions, Soft Matter 8 (35) (2012) 9235–9245.
[37] W. Zhang, B. Han, X. Lai, C. Xiao, S. Xu, X. Meng, Z. Li, J. Meng, T. Wen, X. Yang, J. Liu, H. Xu, Stiffness of cationized gelatin nanoparticles is a key factor determining RNAi efficiency in myeloid leukemia cells, Chem. Commun. 56 (8) (2020) 1255–1258.
[38] V. Kozlovskaya, M. Dolmat, E. Kharlampieva, Polymeric particulates of controlled rigidity for biomedical applications, ACS Appl. Polym. Mater. 3 (5) (2021) 2274–2289.
[39] Z. Li, Y. Zheng, H. Shi, H. Xie, Y. Yang, F. Zhu, L. Ke, H. Chen, Y. Gao, Convenient tuning of the elasticity of self-assembled nano-sized triterpenoids to regulate their biological activities, ACS Appl. Mater. Interfaces (2021).
[40] G. Caldero, M.J. Garcia-Celma, C. Solans, Formation of polymeric nano-emulsions by a low-energy method and their use for nanoparticle preparation, J. Colloid Inter. Sci. 353 (2) (2011) 406–411.
[41] C. Solans, I. Sole, Nano-emulsions: Formation by low-energy methods, Curr. Opin. Colloid 17 (5) (2012) 246–254.
[42] C. Fornaguera, G. Caldero, C. Solans, Electrolytes as a tuning parameter to control nanoemulsion and nanoparticle size, Rsc Adv. 6 (63) (2016) 58203–58211.
[43] C. Fornaguera, A. Dols-Perez, G. Caldero, M.J. Garcia-Celma, J. Camarasa, C. Solans, PLGA nanoparticles prepared by nano-emulsion templating using low-energy methods as efficient nanocarriers for drug delivery across the blood-brain barrier, J. Control Release 211 (2015) 134–143.
[44] E. Soler Besumbes, C. Fornaguera, M. Monge, M.J. García-Celma, J. Carrión, C. Solans, A. Dols-Perez, PLGA cationic nanoparticles, obtained from nano-emulsion templating, as potential DNA vaccines, Eur. Polym. J. 120 (2019), 109229.
[45] S. Leitner, C. Solans, M.J. García-Celma, G. Calderó, Low-energy nano-emulsification approach as a simple strategy to prepare positively charged ethylcellulose nanoparticles, Carbohydr. Polym. 205 (2019) 117–124.
[46] C. Fornaguera, N. Feiner-Gracia, G. Caldero, M.J. Garcia-Celma, C. Solans, Galantamine-loaded PLGA nanoparticles, from nano-emulsion templating, as novel advanced drug delivery systems to treat neurodegenerative diseases, Nanoscale 7 (28) (2015) 12076–12084.
[47] C. Fornaguera, N. Feiner-Gracia, G. Caldero, M.J. Garcia-Celma, C. Solans, PLGA nanoparticles from nano-emulsion templating as imaging agents: Versatile technology to obtain nanoparticles loaded with fluorescent dyes, Colloid Surf. B 147 (2016) 201–209.
[48] C. Fornaguera, N. Feiner-Gracia, A. Dols-Perez, M.J. Garcia-Celma, C. Solans, Versatile Methodology to Encapsulate Gold Nanoparticles in PLGA Nanoparticles Obtained by Nano-Emulsion Templating, Pharm. Res-Dordr. 34 (5) (2017) 1093–1103.
[49] G. Caldero, C. Fornaguera, L. Zadoina, A. Dols-Perez, C. Solans, Design of parenteral MNP-loaded PLGA nanoparticles by a low-energy emulsification approach as theragnostic platforms for intravenous or intratumoral administration, Colloid Surf. B 160 (2017) 535–542.
[50] C. Fornaguera, S. Grijalvo, M. Galan, E. Fuentes-Paniagua, F.J. de la Mata, R. Gomez, R. Eritja, G. Caldero, C. Solans, Novel non-viral gene delivery systems composed of carbosilane dendron functionalized nanoparticles prepared from nano-emulsions as non-viral carriers for antisense oligonucleotides, Int J. Pharm. 478 (1) (2015) 113–123.
[51] N. Feiner-Gracia, A. Dols-Perez, M. Royo, C. Solans, M.J. Garcia-Celma, C. Fornaguera, Cell penetrating peptide grafting of PLGA nanoparticles to enhance cell uptake, Eur. Polym. J. 108 (2018) 429–438.
[52] M. Galan, C. Fornaguera, P. Ortega, G. Caldero, R. Lorente, J.L. Jimenez, J. de la Mata, M.A. Munoz-Fernandez, C. Solans, R. Gomez, Dendronized PLGA nanoparticles with anionic carbosilane dendrons as antiviral agents against HIV infection, Rsc Adv. 6 (77) (2016) 73817–73826.
[53] S. Leitner, S. Grijalvo, C. Solans, R. Eritja, M.J. García-Celma, G. Calderó, Ethylcellulose nanoparticles as a new "in vitro" transfection tool for antisense oligonucleotide delivery, Carbohydr. Polym. 229 (2020), 115451.
[54] S. Leitner, C. Solans, M.J. García-Celma, G. Morral-Ruíz, P. Melgar-Lesmes, G. Calderó, Ethylcellulose nanoparticles prepared from nano-emulsion templates as new folate binding haemocompatible platforms, Mater. Sci. Eng.: C. 120 (2021), 111682.
[55] C. Fornaguera, M. Guerra-Rebollo, M. Ángel Lázaro, C. Castells-Sala, O. Meca-Cortés, V. Ramos-Pérez, A. Cascante, N. Rubio, J. Blanco, S. Borrós, mRNA delivery

system for targeting antigen-presenting cells in vivo, Adv. Health Mater. 7 (17) (2018), 1800335.
[56] C. Fornaguera, M. Llinas, C. Solans, G. Caldero, Design and in vitro evaluation of biocompatible dexamethasone-loaded nanoparticle dispersions, obtained from nano-emulsions, for inhalatory therapy, Colloid Surf. B 125 (2015) 58–64.
[57] D.J. Müller, D. Fotiadis, S. Scheuring, S.A. Müller, A. Engel, Electrostatically Balanced Subnanometer Imaging of Biological Specimens by Atomic Force Microscope, Biophys. J. 76 (2) (1999) 1101–1111.
[58] I. Horcas, R. Fernandez, J.M. Gomez-Rodriguez, J. Colchero, J. Gomez-Herrero, A. M. Baro, WSXM: a software for scanning probe microscopy and a tool for nanotechnology, Rev. Sci. Instrum. 78 (1) (2007), 013705.
[59] P. Hermanowicz, M. Sarna, K. Burda, H. Gabryś, AtomicJ: an open source software for analysis of force curves, Rev. Sci. Instrum. 85 (6) (2014), 063703.
[60] A. Forgiarini, J. Esquena, C. Gonzalez, C. Solans, Formation of nano-emulsions by low-energy emulsification methods at constant temperature, Langmuir 17 (7) (2001) 2076–2083.
[61] M. Monge, C. Fornaguera, C. Quero, A. Dols-Perez, G. Calderó, S. Grijalvo, M. J. García-Celma, C. Rodríguez-Abreu, C. Solans, Functionalized PLGA nanoparticles prepared by nano-emulsion templating interact selectively with proteins involved in the transport through the blood-brain barrier, Eur. J. Pharm. Biopharm. 156 (2020) 155–164.
[62] P.K. Hansma, J.P. Cleveland, M. Radmacher, D.A. Walters, P.E. Hillner, M. Bezanilla, M. Fritz, D. Vie, H.G. Hansma, C.B. Prater, J. Massie, L. Fukunaga, J. Gurley, V. Elings, Tapping mode atomic force microscopy in liquids, Appl. Phys. Lett. 64 (13) (1994) 1738–1740.
[63] C.A.J. Putman, K.O.Vd Werf, B.G.D. Grooth, N.F.V. Hulst, J. Greve, Tapping mode atomic force microscopy in liquid, Appl. Phys. Lett. 64 (18) (1994) 2454–2456.
[64] I. Lee, K. Akiyoshi, Single molecular mechanics of a cholesterol-bearing pullulan nanogel at the hydrophobic interfaces, Biomaterials 25 (15) (2004) 2911–2918.
[65] A. Calò, M. Sanmartí-Espinal, P. Iavicoli, M.-A. Persuy, E. Pajot-Augy, G. Gomila, J. Samitier, Diffusion-controlled deposition of natural nanovesicles containing G-protein coupled receptors for biosensing platforms, Soft Matter 8 (46) (2012) 11632–11643.
[66] M. Di Muzio, R. Millan-Solsona, A. Dols-Perez, J.H. Borrell, L. Fumagalli, G. Gomila, Dielectric properties and lamellarity of single liposomes measured by in-liquid scanning dielectric microscopy, J. Nanobiotechnol. 19 (1) (2021) 167.
[67] R.V.S.P. Sanka, B. Krishnakumar, Y. Leterrier, S. Pandey, S. Rana, V. Michaud, Soft self-healing nanocomposites, Front. Mater. 6 (137) (2019).
[68] Y. Yang, X. Ding, M.W. Urban, Chemical and physical aspects of self-healing materials, Prog. Polym. Sci. 49–50 (2015) 34–59.
[69] P. Guo, D. Liu, K. Subramanyam, B. Wang, J. Yang, J. Huang, D.T. Auguste, M. A. Moses, Nanoparticle elasticity directs tumor uptake, Nat. Commun. 9 (1) (2018) 130.
[70] X. Liang, G. Mao, K.Y. Ng, Mechanical properties and stability measurement of cholesterol-containing liposome on mica by atomic force microscopy, J. Colloid Interface Sci. 278 (1) (2004) 53–62.
[71] M.A. Brady, A. Renzing, T.E.L. Douglas, Q. Liu, S. Wille, M. Parizek, L. Bacakova, A. Kromka, M. Jarosova, G. Godier, P.H. Warnke, Development of Composite Poly (Lactide-co-Glycolide)-Nanodiamond Scaffolds for Bone Cell Growth, J. Nanosci. Nanotechnol. 15 (2) (2015) 1060–1069.
[72] Y. Hui, X. Yi, F. Hou, D. Wibowo, F. Zhang, D. Zhao, H. Gao, C.-X. Zhao, Role of nanoparticle mechanical properties in cancer drug delivery, ACS Nano 13 (7) (2019) 7410–7424.
[73] A.P. Perrino, R. Garcia, How soft is a single protein? The stress–strain curve of antibody pentamers with 5 pN and 50 pm resolutions, Nanoscale 8 (17) (2016) 9151–9158.
[74] G. Gillies, C.A. Prestidge, Interaction forces, deformation and nano-rheology of emulsion droplets as determined by colloid probe AFM, Adv. Colloid Interface Sci. 108–109 (2004) 197–205.
[75] M. Lundqvist, J. Stigler, G. Elia, I. Lynch, T. Cedervall, K.A. Dawson, Nanoparticle size and surface properties determine the protein corona with possible implications for biological impacts, Proc. Natl. Acad. Sci. 105 (38) (2008) 14265.
[76] S.M. Pustulka, K. Ling, S.L. Pish, J.A. Champion, Protein nanoparticle charge and hydrophobicity govern protein corona and macrophage uptake, ACS Appl. Mater. Interfaces 12 (43) (2020) 48284–48295.